Scientific Research Publishing

Materials Sciences and Applications, 2024, 15, 305-319
https://www.scirp.org/journal/msa
ISSN Online: 2153-1188
ISSN Print: 2153-117X

Study the Structural, Electronic, Optical Properties of CZTS Compound after Doping Ba at Zn Site and Si at Sn Site Using Density Functional Theory (DFT)

Fatema Najrin[1], Rabeya Bakar Sarna[1], Sayedul Hasan[2], Shariful Islam[1], Budrun Neher[1], Md. Mahbubur Rahman Bhuiyan[1]*, Farid Ahmed[1]

[1]Department of Physics, Jahangirnagar University, Bangladesh
[2]Department of Physics, Sunamganj Science and Technology University, Santiganj, Bangladesh
Email: *bhuiyanphysics@juniv.edu, *rahmanmahbubur@ymail.com

How to cite this paper: Najrin, F., Sarna, R.B., Hasan, S., Islam, S., Neher, B., Bhuiyan, Md.M.R. and Ahmed, F. (2024) Study the Structural, Electronic, Optical Properties of CZTS Compound after Doping Ba at Zn Site and Si at Sn Site Using Density Functional Theory (DFT). *Materials Sciences and Applications*, **15**, 305-319.
https://doi.org/10.4236/msa.2024.159021

Received: June 11, 2024
Accepted: September 8, 2024
Published: September 11, 2024

Abstract

The structural, electronic, and optical properties of $Cu_2Zn_{1-x}Ba_xSn_{1-y}Si_yS_4$ compounds have been calculated using GGA-PBE function within the framework of Density Functional Theory (DFT). In the present work, lattice parameters remained the same, that is tetragonal crystal structure for 0% and 100% doping concentration. The electronic band gap of $Cu_2Zn_{1-x}Ba_xSn_{1-y}Si_yS_4$ compounds has been gradually increased for continuous increment of doping concentration where the highest electronic band gap is 1.117 eV for Cu_2BaSiS_4 structure. Moreover, the band gap changes from direct to indirect band gap with the increase of doping concentration in the parent compound. The absorption coefficient has been found to be high ($> 10^4$ cm^{-1}) in UV-region for all the doping concentration which makes the studied compound as a potential candidate of absorber layer in the UV detector. The theoretical study of the effect of double doping in the CZTS compound is very interesting for improving the quality of it and it would be a reference for the theoretical and experimental researchers.

Keywords

Photovoltaics, Absorber Layer, Density Functional Theory (DFT), Band Gap, Solar Cell

1. Introduction

Nowadays scientists and technologists have been replacing fossil fuels with renewable

energy sources such as photovoltaic solar energy in order to deal with the discharge of greenhouse gases that resulting climate change on the earth [1]-[3] whereas photovoltaic conversion system provides renewable and eco-friendly energy [4]. Past few years CdTe [5], CIGS [5]-[7] and CZTS have gained interest as an application in photovoltaic solar cells and these materials have conversion power efficiency between 16% - 20% to date [4] [8] which making them conventional semiconductor materials. But the existence of harmful elements like In and Ga in CIGS has raised global concern and on the other hand, CZTS has been increased interest due to its low cost, non-toxic, eco-friendliness nature [9]-[13] and including application in solar cell [14] [15]. The CZTS thin films have a high level of optical absorption coefficient ($>10^4$ cm^{-1}) [6] [7] [16] [17] as well as p-type conductivity and a direct band gap.

In 2010, Persson *et al*. investigated the electrical structures and optical features of Kesterite (KS) and Stannite (ST) types Cu_2ZnSnS_4 and $Cu_2ZnSnSe_4$ where they found direct band gap and high absorption coefficient ($>10^4$ cm^{-1}) for KS-type using density functional theory [18]. In 2015, Kong *et al*. investigated the electronic and optical properties of Kesterite and Stannite Cu_2ZnSnS_4 using the DFT theory where they reported that the optical properties of CZTS weak dependency of Cu, Zn cation ordering and these materials have higher potentiality for photovoltaics due to their large light absorption coefficient [19]. In 2015, AN Rosli *et al*. suggested that the band structure of KS-Type CZTS where they found the band gap of KS-type CZTZ has been shown semiconductor nature [20]. Compared to the pristine structure, doping with different atoms is an appropriate approach to develop the physicochemical properties [21]. However, to convert light energy into photoelectricity and improve the photovoltaic solar cell's properties, the p-n junction must be improved [22]. In 2020, N. Manavizadeh *et al*. investigated the effect of Bi-doping on CZTS using density functional theory, and they reported that the Bi-doped structure had a high absorption coefficient ($>10^4$ cm^{-1}) in the visible region but the pure structure did not have this [23]. Using thermal evaporation method, M. Marzougiet *et al*. studied the structural, optical properties of Na-doping on CZTS and they found direct band gap with absorption coefficient in the UV-region at 5% Na-doping concentration on CZTS [24]. Using DFT, C. Tablero *et al*. studied the effect of the oxygen isoelectronic substitution in CZTS and they reported O-doped CZTS has an electrical structure that includes a subband towards the CB. This deeper band is comprised of the Sn-5s and O-2p orbitals [25].

The quantum mechanical approach enables us to make more accurate predictions regarding the behavior of particles when we attempt to interact with them. We are inspired to perform such a theoretical investigation utilizing the quantum mechanical approach based on DFT to analyze the structural, electronic and optical properties of the CZTS compounds. As far as we are aware, theoretical and experimental research has been done by single doping but double doping in CZTS compound and their structural, electronic and optical properties are still unknown

to us. Therefore, we are interested to dope Ba at Zn-site and to dope Si at Sn-site resulting the $Cu_2Zn_{1-x}Ba_xSn_{1-y}Si_yS_4$ compound and to characterize the structural, electronic, and optical characteristics of $Cu_2Zn_{1-x}Ba_xSn_{1-y}Si_yS_4$ compounds using the DFT based calculation. Moreover, Ba and Si have been chosen for their semiconductor nature, which might increase the useability of the $Cu_2Zn_{1-x}Ba_xSn_{1-y}Si_yS_4$ compound as an absorber layer in solar cells.

2. Computational Details

To investigate the structural, electronic and optical properties of $Cu_2Zn_{1-x}Ba_xSn_{1-y}Si_yS_4$ (where x, y = 0.00, 0.25, 0.50, 0.75, 1.00), the CASTEP (Cambridge Serial Total Energy Package, Material Studio 2017) code was used to execute quantum mechanical approach density functional theory (DFT) [26]-[29] simulation which was based on a nonlocal ultrasoft pseudopotential [30] that indicate the presence of firmly bonded core electrons and to illustrate the electron-ion interaction. To find the exchange correlation, the Perdew-Burke-Ernzerhof (PBE) [31] form of the generalized gradient approximation (GGA) was used with a plane-wave cut-off energy of 500 eV to get comprehensive solution along with default medium level of self-consistent field (SCF) tolerance in the program [32]. To conduct the computation, we constructed a supercell measuring 2 × 1 × 1, and The BFGS algorithm [33] was employed to optimize the crystal structure through the minimization of both total energy and internal forces. The KS-type $Cu_2Zn_{1-x}Ba_xSn_{1-y}Si_yS_4$ compounds, where x and y represent doping concentration, have been studied using a Monkhorst Pack scheme [34]. The calculations were performed using a 2 × 4 × 2 k-point mesh size. We selected 1000 cycles, which is sufficient to optimize every structure. The structural parameters of the CZTS (pure and doped) were calculated using the Broyden-Fletcher-Goldfarb-Shanno (BFGS) algorithm with energy change per atom less than 2×10^{-5} eV, residual force less than 0.05 eV/Å, stress below 0.1GPa, and atom displacement during geometry optimization less than 0.002Å.

In order to find the structural stability, the formation energy is obtained by using the formula [35]:

$$E_{for} = E_{Cu_2Zn_{1-x}Ba_xSn_{1-y}Si_yS_4} - \left(E_{Cu} \times 2 + E_{Zn} \times (1-x) + E_{Ba} \times x + E_{Sn} \times (1-y) + E_{Si} \times y + E_S \times 4\right) \quad (1)$$

whereas $E_{Cu_2Zn_{1-x}Ba_xSn_{1-y}Si_yS_4}$ determined the ground state energy of the structures, E_{Cu}, E_{Zn}, E_{Ba}, E_{Sn}, E_S determines the energy of Cu, Zn, Ba, Sn, Si, S atoms respectively.

To get optical properties, the complex dielectric function is represented as

$$\varepsilon(\omega) = \varepsilon_1(\omega) + i\varepsilon_2(\omega) \quad (2)$$

The real portion of dielectric constant $\varepsilon_1(\omega)$ affects light polarization and absorption within a material under external electric field impact. The imaginary portion of dielectric constant $\varepsilon_2(\omega)$ represents the loss of molecular polarization due to variations in the external electric field. Dielectric function reveals solid's band

structure and spectral information [36].

Refractive index can be expressed as a frequency-dependent complex function,

$$N(\omega) = n(\omega) + i\kappa(\omega) \tag{3}$$

where $n(\omega)$ represents the refractive index and $k(\omega)$ represents the extinction index. These values have been determined by analyzing the real and imaginary parts of the dielectric function, as mentioned previously [37].

3. Result and Discussion

3.1. Structural Properties

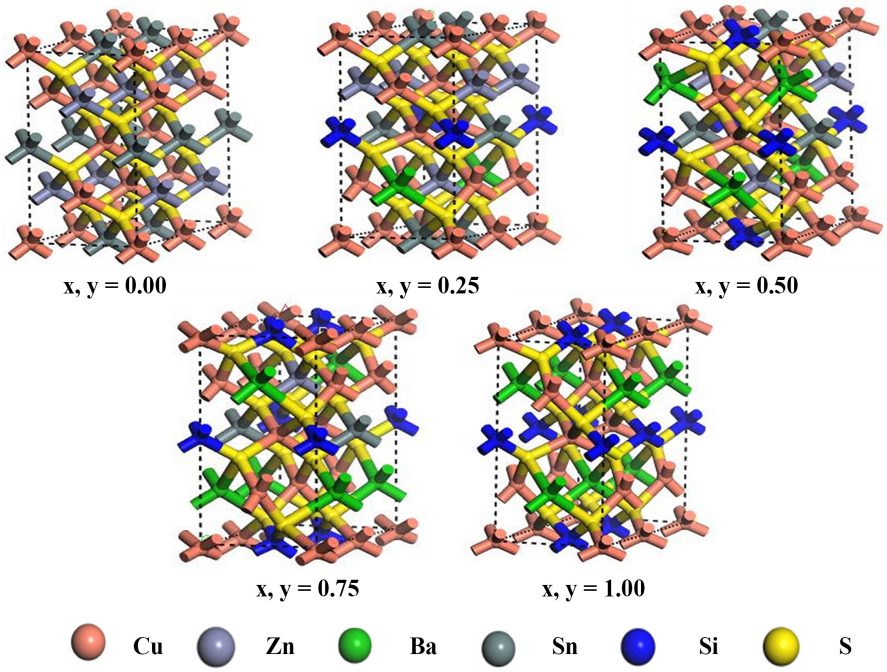

Figure 1. Optimized crystal structure of $Cu_2Zn_{1-x}Ba_xSn_{1-y}Si_yS_4$ compounds for different doping concentration (x, y).

In this study, all the structures of $Cu_2Zn_{1-x}Ba_xSn_{1-y}Si_yS_4$ compounds have been optimized to study different properties at low ground state energy to get a more stable form of the structures. According to optimized structures, it has been observed that KS-type (space group: $I\bar{4}$ #no: 82) pure and 100% doped (x, y = 1.00) CZTS compound with body centered tetragonal crystal structure. The optimized crystal structures of the $Cu_2Zn_{1-x}Ba_xSn_{1-y}Si_yS_4$ compounds have been depicted in **Figure 1** in which the Wyckoff position of four Cu atoms are 2a and 2c location, of two Zn atom at 2d, of two Sn atoms at 2b, and of eight anions S atom at 8g for both pure and doped CZTS compound is comparable to C. Persson *et al.* [38]. The lattice parameters, cell volumes, ground state energy, and formation energy have been summarized in **Table 1**. The lattice parameter of KS-type Cu_2ZnSnS_4 (x, y = 0.00) structure are a = 5.47Å, b = 5.47 Å, and c = 10.94 Å in the present studied structural optimization [39]-[41]. It has been shown that for x, y = 0.00, the value

of c/a > 2 which is similar to A. Ghosh *et al.* [42] but in experimental condition the value c/a < 2 due to Cu/Zn disorder [38]. With gradual increase in doping concentration, the effect of change in lattice parameters has been observed. Due to the increase in doping concentration, 0% and 100% doped structures have remained in the tetragonal crystal structure, but for 25%, 50%, and 75% doped structures, they have shown variations in deformation from their original crystal structure.

Table 1. Summarized lattice parameters, cell volumes, ground state energy, and formation energy of $Cu_2Zn_{1-x}Ba_xSn_{1-y}Si_yS_4$ compound after geometrical optimization using DFT based calculation.

$Cu_2Zn_{1-x}Ba_xSn_{1-y}Si_yS_4$							
Phase	Doping concentration (x, y)	Lattice parameter (Å)			Volume (Å^3)	Ground state of energy (eV)	Formation Energy (eV)
		A	b	c			
KS	0.00	5.47	5.47	10.94	654.60	−23496.35	−15.38
	0.25	5.44	5.50	11.21	670.65	−22499.83	−17.72
	0.50	5.42	5.56	11.29	680.83	−21503.75	−20.52
	0.75	5.56	5.67	11.22	706.77	−20507.34	−22.98
	1.00	5.62	5.62	11.43	723.26	−19591.08	−105.60

A lower formation energy indicates greater stability, and negative values suggest spontaneous formation which is given in Equation 1 [43]. The value of formation energies has been found in an increment nature with increasing doping concentration which reveals that the stability of the compound gradually increased with doping concentration.

For various cation (Cu, Zn, Ba, Sn, Si, S), distance from anion S for nearby cations are different. The average bond length of S-Cu, S-Zn, S-Ba, S-Sn, S-Si are gradually increased with doping concentration which is also presented in **Table 2**. The increment of bond length indicates that the atomic arrangement changes with increasing impurities. Electronic configuration changes electron-nuclei interactions which ultimately affect bond lengths.

Table 2. Summarized bond length of $Cu_2Zn_{1-x}Ba_xSn_{1-y}Si_yS_4$ compound after geometrical optimization using DFT based calculation.

$Cu_2Zn_{1-x}Ba_xSn_{1-y}Si_yS_4$					
Bond	Doping concentration (x, y)				
	0.00	0.25	0.50	0.75	1.00
S-Cu	2.32	2.34	2.36	2.40	2.42
S-Zn	2.36	2.38	2.37	2.38	-
S-Sn	2.48	2.49	2.52	2.50	-
S-Si	-	2.17	2.16	2.16	2.17
S-Ba	-	2.92	2.95	2.94	2.94

3.2 Electronic Properties

The band structures have been understandable for $Cu_2Zn_{1-x}Ba_xSn_{1-y}Si_yS_4$ compound with the symmetry point of Brillouin zone ($G \rightarrow F \rightarrow Q \rightarrow Z \rightarrow G$) which is shown in Figure 2 for both pure and doped CZTS compounds. The Brillouin zone is a periodic representation of the structure of crystal in reciprocal space which is important for studying electronic band structures and predicting material properties [44]. The summarized band gap and their type in the studied compound has also been presented in Table 3.

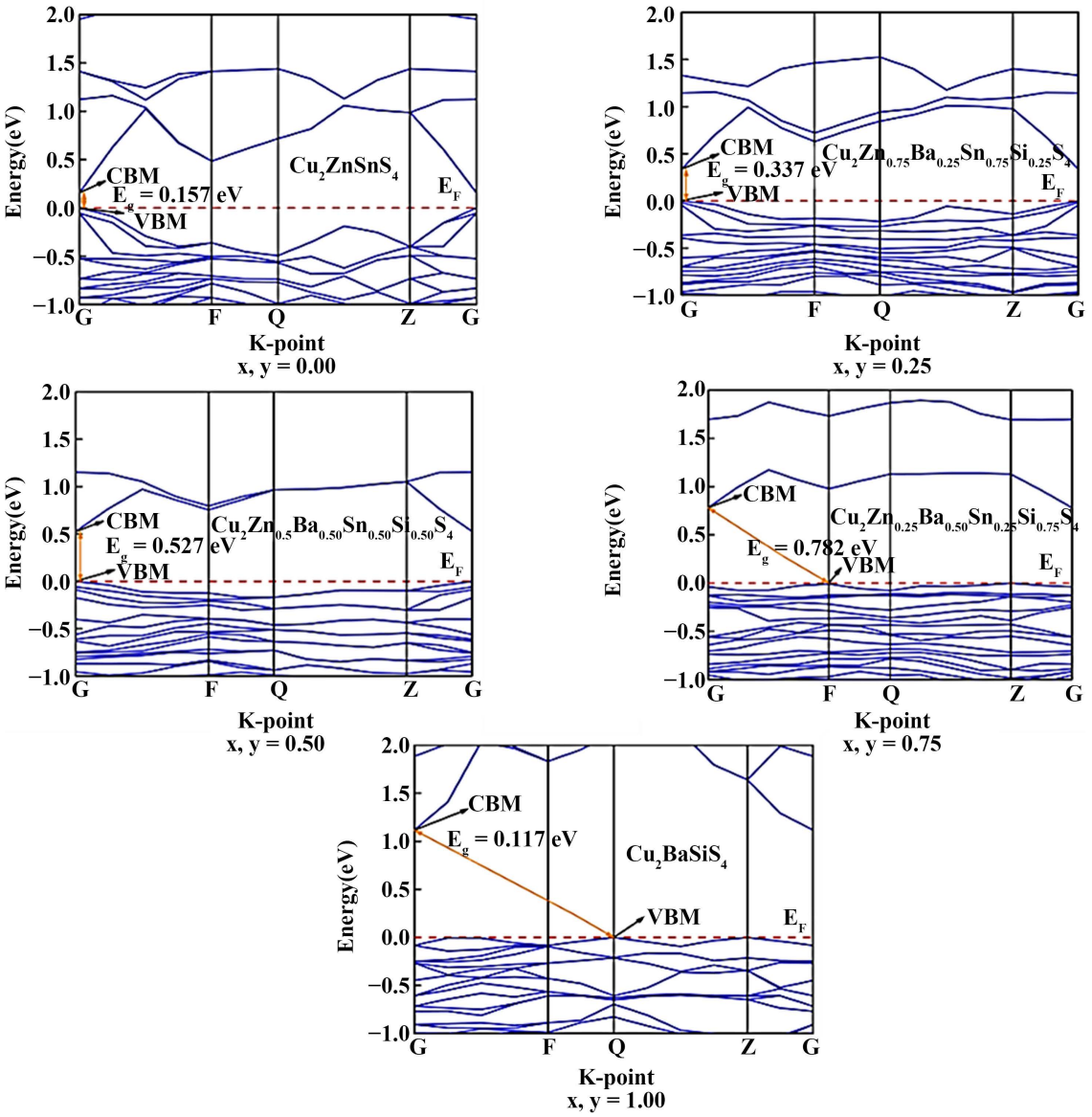

Figure 2. Calculated band structures of $Cu_2Zn_{1-x}Ba_xSn_{1-y}Si_yS_4$ compound.

The Fermi levels (E_F) have been depicted in Figure 2 for pure and doped structures. The band gaps are modified using a scissors operator based on experimental data because the GGA underestimates conduction band state energy and typically

exceeds it [45] [46]. According to Figure 2, the concentrations of doping x, y = 0.00, 0.25, and 0.50 show that the conduction band minimum (CBM) and valence band maximum (VBM) are located at the "G" K-point. This indicates that the electronic band gap of these structures is direct. Whereas for doping concentration x, y = 0.75 and 1.00, the conduction band minimum (CBM) has been occurred at "G" K-point for doping concentration x, y = 0.75 and 1.00 and the valence band maximum (VBM) have been situated at "F" K-point and "Q" K-point for doping concentration x, y = 0.75 and 1.00 respectively which signified that the electronic band gaps have been shown indirect nature. This study has revealed that the band gap for pure structure is 0.157 eV which is relevant with reference value of 0.16 eV [47] from recent GGA-PBE calculation. The electronic band gaps have been shown to increase in nature with the gradual increment of doping concentration as depicted in Figure 3.

Table 3. Summarized bandgap (eV) and the nature of band of $Cu_2Zn_{1-x}Ba_xSn_{1-y}Si_yS_4$ compound.

$Cu_2Zn_{1-x}Ba_xSn_{1-y}Si_yS_4$		
Doping concentration (x, y)	Bandgap (eV)	Bandgap type
0.00	0.157	Direct
0.25	0.337	Direct
0.50	0.527	Direct
0.75	0.782	Indirect
1.00	1.117	Indirect

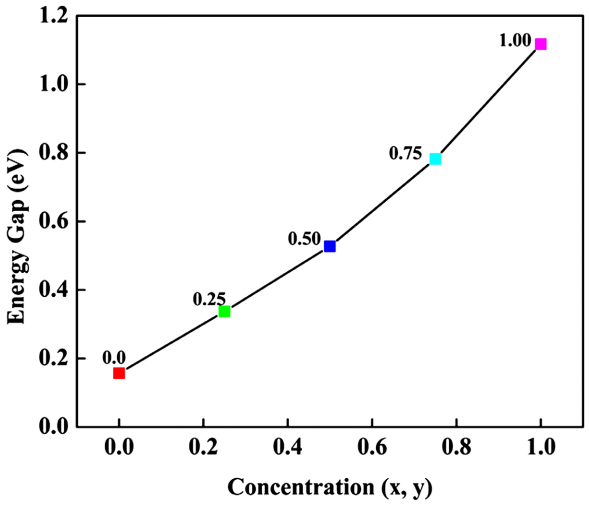

Figure 3. The variation of energy gap that caused by Ba and Si concentration in $Cu_2Zn_{1-x}Ba_xSn_{1-y}Si_yS_4$

A high DOS means more than one occupation state at a certain amount of energy. The total density of state (TDOS) and partial density of state (PDOS) have been described in Figure 4 for all the structures. In pure structures (at x, y = 0.00),

the maximum valence band are constructed via hybridization of 3d state of Cu, 3d state of Zn and 3p state of S; whereas the minimum conduction band form from 3p state of S and 5s of Sn states [48].

After increasing impurities, it has been revealed that the VBMs (valance band maximum) are mainly formed from Cu-3d and the CBMs are constructed by S-3p. This means that the changing composition of quaternary structures from Zn to Ba and Sn to Si do not influence enough main feature of energy distributions of Cu-3d and S-3p. A structure must be categorized as a semiconductor if it has a fully occupied valence band and a maximum unoccupied conduction band.

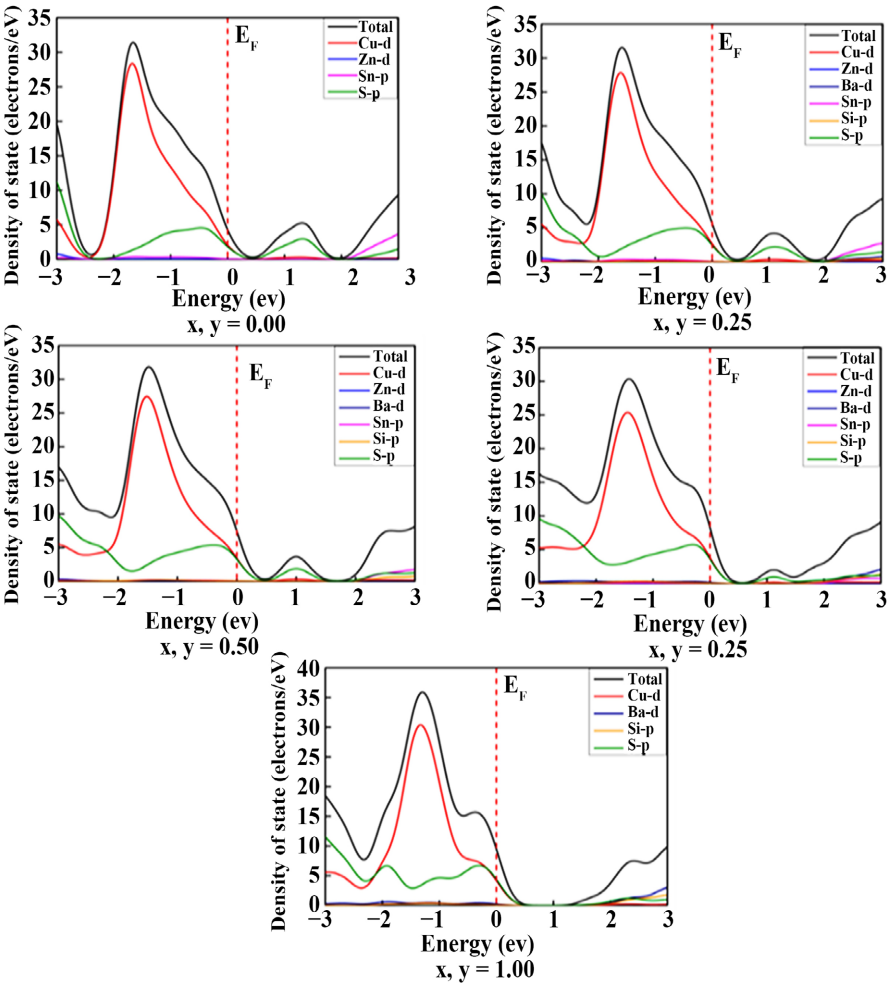

Figure 4. Total and partial density of state of $Cu_2Zn_{1-x}Ba_xSn_{1-y}Si_yS_4$ compound for different doping concentration (x, y).

3.3 Optical Properties

The optical properties of a solid are directly influenced by the ground state electrical structure. **Figure 5** and **Figure 6** show the optical properties of pure and doped CZTS materials for photon energy up to 20 eV. It is obvious that all optical properties depend on photon frequency.

Absorption coefficients of $Cu_2Zn_{1-x}Ba_xSn_{1-y}Si_yS_4$ compounds have been observed

in UV region and visible region as shown in **Figure 5(a)**. The highest peaks have been placed at 9.8 eV, 9.6 eV, 8.31 eV, 8.6 eV, 8.9 eV for x, y = 0.00, 0.25, 0.50, 0.75, 1.00 doping concentration, respectively. It has been observed that the major peaks have been shifted towards lower energies when doping concentrations have gradually increased. Absorption coefficient for all the structures has been observed with a larger value (>10^4 cm^{-1}) [49].

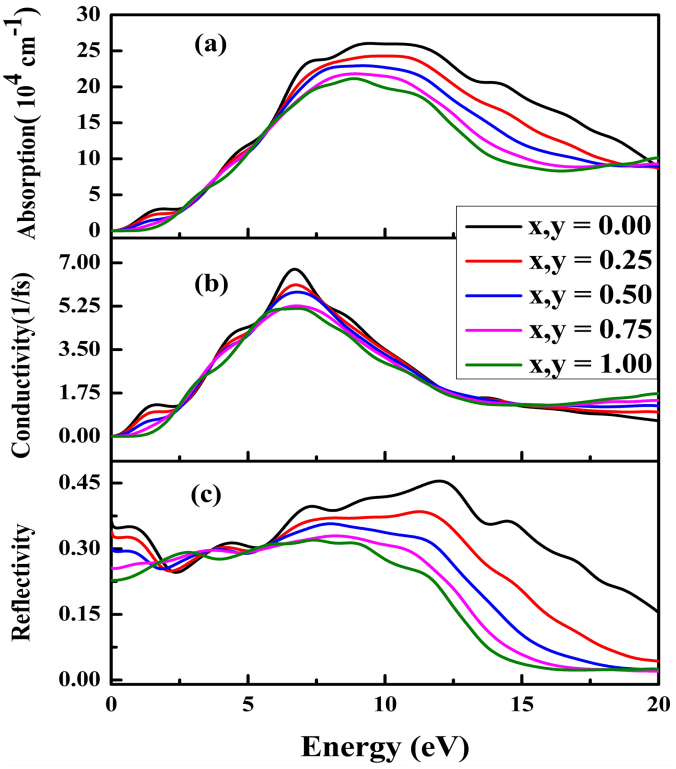

Figure 5. Effect of variation of (a) absorption coefficient, (b) optical conductivity, and (c) reflectivity with the change of energy for $Cu_2Zn_{1-x}Ba_xSn_{1-y}Si_yS_4$ compound.

The optical conductivity spectrum refers to the amount of free charge carriers generated by bond breaking down during electron-photon interaction [50]. The optical conductivity has been depicted in **Figure 5(b)** for both pure and doped CZTS compound. The major peaks have been placed at 6.7 eV, 6.7 eV, 6.8 eV, 6.9 eV, 6.9 eV for x, y = 0.00, 0.25, 0.50, 0.75, 1.00 doping concentration of $Cu_2Zn_{1-x}Ba_xSn_{1-y}Si_yS_4$ compounds, respectively. The OCs (optical conductivity) have been gradually decreasing with increasing doping concentration.

Reflectivity always varies from 0 to 1. Absorption of light is closely related to reflectivity. The reflectivity has been presented in **Figure 5(c)** for both pure and doped CZTS compounds. It seems that the pure CZTS has the lowest reflectivity at visible and IR-region [51]. The IR and visible regions have lower reflectivity, while the UV region has better reflectivity. With the increment of doping concentration, the reflectivity has shown a lower value than pure CZTS.

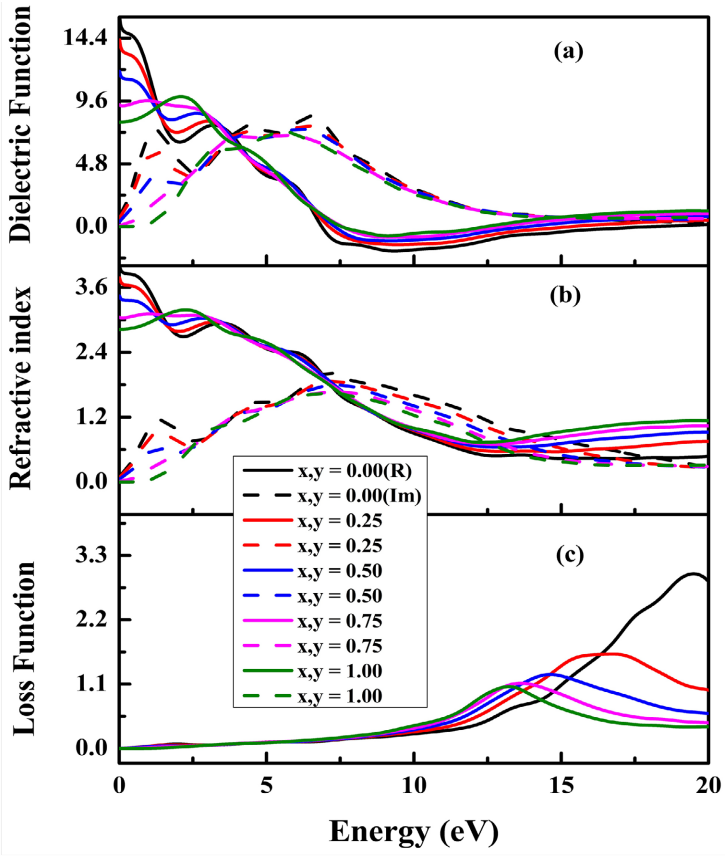

Figure 6. Effect of variation of (a) dielectric function, (b) refractive index, and (c) loss function with the change of energy for $Cu_2Zn_{1-x}Ba_xSn_{1-y}Si_yS_4$ compound.

Figure 6(a) shows a real and imaginary part of the dielectric function plotted against energy for $Cu_2Zn_{1-x}Ba_xSn_{1-y}Si_yS_4$ compound. To understand how materials absorb electricity, it is necessary to know about the imaginary part of the dielectric function. The absorption of material is significant when the absorptive component of the electronic dielectric function $\varepsilon_2(\omega)$ has a large value. The first threshold point has occurred at 0.09 eV, 0.13 eV, 0.21 eV, 0.54 eV,1.02 eV for x, y = 0.00, 0.25, 0.50, 0.75 and 1.00 doping concentration, respectively which means the threshold for direct optical transition between high valence and low conduction bands in this calculation and the principal peaks of imaginary part of the dielectric function have been observed at 6.52 eV, 6.50 eV, 6.15 eV, 5.65 eV, 5.62 eV for x, y = 0.00, 0.25, 0.50, 0.75 and 1.00 doping composition respectively which suggests that these materials could be applied as a UV-detector or LED detector [52]. Fig. 5(a) has shown differing minor peaks in the 0 - 20 eV energy range due to inter-band transitions between the valence and conduction bands. Real parts of dielectric functions could be determined using the Kramer-Kronig relationship [53]. The static dielectric function has occurred at 3.25 eV, 3.08 eV, 2.62 eV, 2.40 eV, 2.09 eV for x, y = 0.00, 0.25, 0.50, 0.75, 1.00 doping concentration, respectively. The Penn relation ($\varepsilon_1(0) \approx 1+(\hbar\omega/Eg)^2$) suggested that the static dielectric constant

of a material decreases with an increase in bandgap, and vice versa [54]. The maximum peak has been found at 0 eV, 0 eV, 0 eV, 0.96 eV and 2.09 eV and real part of the dielectric function has become zero at 6.87eV, 7.12eV, 7.32eV, 7.57 eV, 7.53 eV for x, y = 0.00, 0.25, 0.50, 0.75, 1.00 doping concentration, respectively. As energy increases, the dielectric function becomes negative, indicating that the medium fully reflects electromagnetic waves, which suggests its metallic nature.

The refractive function has been plotted against energy which is shown in **Figure 6(b)**. The values of refractive index n (0) are 3.91, 3.65, 3.38, 3.04, 2.82 for x, y = 0.00, 0.25, 0.50, 0.75, 1.00, respectively. The peak value of refractive index was found in the visible region, and it gradually dropped with higher energy scales. Therefore, the refractive index has been decreased with increment of impurities.

The energy loss function spectrum peak indicates plasma resonance, a collective motion of particles, and its corresponding frequency is the plasma frequency [19]. Photon energy above the material bandgap drains compounds. **Figure 6(c)** has been presented that the plasmon peaks arises at 19.43 eV, 16.36 eV, 14.43 eV, 13.50 eV, 13.11 eV for increasing doping concentration.

4. Conclusion

In the present work, the structural, electronic, and optical properties of $Cu_2Zn_{1-x}Ba_xSn_{1-y}Si_yS_4$ compounds have been studied using GGA-PBE functional via DFT analysis. The optimized structural calculation for pure and doped CZTS compound shows that pure and fully doped (x, y = 1) CZTS compound crystallized in tetragonal structure. There are some structural deviations from tetragonal structure in the case of doped structures for x, y = 0.25, 0.5, and 0.75. The change in lattice parameters due to doping has been shown for 0% and 100% doping concentration, the crystal structure remained the same that is tetragonal crystal structure. The electronic band gaps have been increased gradually with the increase of doping concentration in the CZTS compound. The highest band gap has been found for Cu_2BaSiS_4 by 1.117 eV for fully doped CZTS compound. The obtained results for band gap identified that the present studied CZTS compounds are potential candidate as semiconductor. For all the doping concentration, the absorption coefficient is high ($>10^4$ cm^{-1}) in UV-region as result these structures might be used as an absorber layer in UV detector. All the structures have a photoconductive nature with minimal loss function, making them potentially suitable for application in optoelectronic devices (OE). Refractive index and reflectivity indicate significant photon energy loss, which can be enhanced by modifying experimental work. The studied compound is promising, and it should be realized experimentally to verify the theoretical observations.

Data Availability

Data sharing is not applicable to this article as no datasets were generated or analyzed during the current study. (The article describes entirely theoretical research.)

Conflicts of Interest

The authors declare no conflicts of interest regarding the publication of this paper.

References

[1] Mohammadnejad, S. and Baghban Parashkouh, A. (2017) CZTSSe Solar Cell Efficiency Improvement Using a New Band-Gap Grading Model in Absorber Layer. *Applied Physics A*, **123**, Article No. 758. https://doi.org/10.1007/s00339-017-1371-x

[2] Yin, H., Ho, J.K.W., Cheung, S.H., Yan, R.J., Chiu, K.L., Hao, X., *et al*. (2018) Designing a Ternary Photovoltaic Cell for Indoor Light Harvesting with a Power Conversion Efficiency Exceeding 20%. *Journal of Materials Chemistry A*, **6**, 8579-8585. https://doi.org/10.1039/c8ta01728j

[3] Bai, D., Bian, H., Jin, Z., Wang, H., Meng, L., Wang, Q., *et al*. (2018) Temperature-assisted Crystallization for Inorganic $CsPbI_2Br$ Perovskite Solar Cells to Attain High Stabilized Efficiency 14.81%. *Nano Energy*, **52**, 408-415. https://doi.org/10.1016/j.nanoen.2018.08.012

[4] Green, M.A., Emery, K., Hishikawa, Y. and Warta, W. (2010) Solar Cell Efficiency Tables (Version 36). *Progress in Photovoltaics*: *Research and Applications*, **18**, 346-352. https://doi.org/10.1002/pip.1021

[5] Mitchell, K., Fahrenbruch, A.L. and Bube, R.H. (1975) Structure and Electrical Properties of CdS and CdTe Thick Films for Solar Cell Applications. *Journal of Vacuum Science and Technology*, **12**, 909-911. https://doi.org/10.1116/1.568698

[6] Yu, M. (2001) 'In God We Trusted, in China We Busted': The China Commando Group of the Special Operations Executive (SOE). *Intelligence and National Security*, **16**, 37-60. https://doi.org/10.1080/02684520412331306290

[7] Matsushita, H., Maeda, T., Katsui, A. and Takizawa, T. (2000) Thermal Analysis and Synthesis from the Melts of Cu-Based Quaternary Compounds Cu-III-IV-VI_4 and Cu_2-II-IV-VI_4 (II = Zn, Cd; III = Ga, In; IV = Ge, Sn; VI = Se). *Journal of Crystal Growth*, **208**, 416-422. https://doi.org/10.1016/s0022-0248(99)00468-6

[8] Jackson, P., Hariskos, D., Lotter, E., Paetel, S., Wuerz, R., Menner, R., *et al*. (2011) New World Record Efficiency for Cu(In, Ga)Se_2 Thin-Film Solar Cells Beyond 20%. *Progress in Photovoltaics*: *Research and Applications*, **19**, 894-897. https://doi.org/10.1002/pip.1078

[9] Walsh, A., Chen, S., Wei, S. and Gong, X. (2012) Kesterite Thin-film Solar Cells: Advances in Materials Modelling of Cu_2ZnSnS_4. *Advanced Energy Materials*, **2**, 400-409. https://doi.org/10.1002/aenm.201100630

[10] Katagiri, H., Jimbo, K., Maw, W.S., Oishi, K., Yamazaki, M., Araki, H., *et al*. (2009) Development of CZTS-Based Thin Film Solar Cells. *Thin Solid Films*, **517**, 2455-2460. https://doi.org/10.1016/j.tsf.2008.11.002

[11] Barkhouse, D.A.R., Gunawan, O., Gokmen, T., Todorov, T.K. and Mitzi, D.B. (2011) Yield Predictions for Photovoltaic Power Plants: Empirical Validation, Recent Advances and Remaining Uncertainties. *Progress in Photovoltaics*: *Research and Applications*, **20**, 6-11. https://doi.org/10.1002/pip.1160

[12] Wang, H. (2011) Progress in Thin Film Solar Cells Based on Cu_2ZnSnS_4. *International Journal of Photoenergy*, **2011**, Article ID: 801292. https://doi.org/10.1155/2011/801292

[13] Ki, W. and Hillhouse, H.W. (2011) Earth-Abundant Element Photovoltaics Directly from Soluble Precursors with High Yield Using a Non-Toxic Solvent. *Advanced Energy Materials*, **1**, 732-735. https://doi.org/10.1002/aenm.201100140

[14] Fella, C.M., Romanyuk, Y.E. and Tiwari, A.N. (2013) Technological Status of $Cu_2ZnSn(S, Se)_4$ Thin Film Solar Cells. *Solar Energy Materials and Solar Cells*, **119**, 276-277. https://doi.org/10.1016/j.solmat.2013.08.027

[15] Chen, S., Walsh, A., Gong, X. and Wei, S. (2013) Classification of Lattice Defects in the Kesterite Cu_2ZnSnS_4 and $Cu_2ZnSnSe_4$ Earth-Abundant Solar Cell Absorbers. *Advanced Materials*, **25**, 1522-1539. https://doi.org/10.1002/adma.201203146

[16] Scragg, J.J., Dale, P.J. and Peter, L.M. (2008) Towards Sustainable Materials for Solar Energy Conversion: Preparation and Photoelectrochemical Characterization of Cu_2ZnSnS_4. *Electrochemistry Communications*, **10**, 639-642. https://doi.org/10.1016/j.elecom.2008.02.008

[17] Nakazawa, K.I. (1988) Electrical and Optical Properties of Stannite-Type Quaternary Semiconductor Thin Films. *Japanese Journal of Applied Physics*, **27**, 2094. https://doi.org/10.1143/jjap.27.2094

[18] Persson, C. (2010) Electronic and Optical Properties of Cu_2ZnSnS_4 and $Cu_2ZnSnSe_4$. *Journal of Applied Physics*, **107**, Article ID: 053710. https://doi.org/10.1063/1.3318468

[19] Kong, L. and Deng, J.X. (2015) First-Principles Study on Electronic and Optical Properties of Kesterite and Stannite Cu_2ZnSnS_4 Photovoltaic Absorbers. *Materials Science Forum*, **815**, 80-88. https://doi.org/10.4028/www.scientific.net/msf.815.80

[20] Basri, K.N., Zabidi, N.A., Abu Kassim, H. and Rosli, A.N. (2015) Density Functional Theory (DFT) Calculation of Band Structure of Kesterite. *Advanced Materials Research*, **1107**, 491-495. https://doi.org/10.4028/www.scientific.net/amr.1107.491

[21] Rahman, A.U., Neher, B., Hossain, S., Bhuiyan, M.M.R., Saaduzzaman, D.M., Hasan, S.M., *et al*. (2024) A Comparative DFT Investigation on the Structural, Electric, Thermodynamic, and Optical Properties of the Pristine and Various Metals and Nonmetals (Li, Be, B, N, O, and F) Doped Graphene and Silicene Nanosheets. *Physica B: Condensed Matter*, **675**, 415615. https://doi.org/10.1016/j.physb.2023.415615

[22] Tang, Y., Wang, Z., Wang, P., Wu, F., Wang, Y., Chen, Y., *et al*. (2019) WSe_2 Photovoltaic Device Based on Intramolecular p-n Junction. *Small*, **15**, Article ID: 1805545. https://doi.org/10.1002/smll.201805545

[23] Barati, M., Nouri, N. and Manavizadeh, N. (2020). Investigation of Bismuth Doping Effects on CZTS Properties: A Density Functional Theory Study. 2020 28*th Iranian Conference on Electrical Engineering* (*ICEE*), Tabriz, 4-6 August 2020, 1-5. https://doi.org/10.1109/icee50131.2020.9261048

[24] Marzougi, M., Ben Rabeh, M. and Kanzari, M. (2019) Effect of Na Doping on Structural and Optical Properties in Cu_2ZnSnS_4 Thin Films Synthesized by Thermal Evaporation Method. *Thin Solid Films*, **672**, 41-46. https://doi.org/10.1016/j.tsf.2018.12.046

[25] Tablero, C. (2012) Effect of the Oxygen Isoelectronic Substitution in Cu_2ZnSnS_4 and Its Photovoltaic Application. *Thin Solid Films*, **520**, 5011-5013. https://doi.org/10.1016/j.tsf.2012.03.020

[26] Segall, M.D., Lindan, P.J.D., Probert, M.J., Pickard, C.J., Hasnip, P.J., Clark, S.J., *et al*. (2002) First-Principles Simulation: Ideas, Illustrations and the CASTEP Code. *Journal of Physics: Condensed Matter*, **14**, 2717-2744. https://doi.org/10.1088/0953-8984/14/11/301

[27] Kohn, W. and Vashishta, P. (1983) General Density Functional Theory. In: Lundqvist, S. and March, N.H., Eds., *Theory of the Inhomogeneous Electron Gas*, Springer, 79-147. https://doi.org/10.1007/978-1-4899-0415-7_2

[28] Kohn, W. and Sham, L.J. (1965) Self-Consistent Equations Including Exchange and Correlation Effects. *Physical Review*, **140**, A1133-A1138. https://doi.org/10.1103/physrev.140.a1133

[29] Clark, S.J., Segall, M.D., Pickard, C.J., Hasnip, P.J., Probert, M.I.J., Refson, K., *et al.* (2005) First Principles Methods Using CASTEP. *Zeitschrift für Kristallographie—Crystalline Materials*, **220**, 567-570. https://doi.org/10.1524/zkri.220.5.567.65075

[30] Vanderbilt, D. (1990) Soft Self-Consistent Pseudopotentials in a Generalized Eigenvalue Formalism. *Physical Review B*, **41**, 7892-7895. https://doi.org/10.1103/physrevb.41.7892

[31] Perdew, J.P., Burke, K. and Ernzerhof, M. (1996) Generalized Gradient Approximation Made Simple. *Physical Review Letters*, **77**, 3865-3868. https://doi.org/10.1103/physrevlett.77.3865

[32] McWeeny, R. (1968) Multi-Configuration SCF Calculations. *Symposia of the Faraday Society*, **2**, 7-14. https://doi.org/10.1039/sf9680200007

[33] Fischer, T.H. and Almlof, J. (1992) General Methods for Geometry and Wave Function Optimization. *The Journal of Physical Chemistry*, **96**, 9768-9774. https://doi.org/10.1021/j100203a036

[34] Pack, J.D. and Monkhorst, H.J. (1977) "Special Points for Brillouin-Zone Integrations"—A Reply. *Physical Review B*, **16**, 1748-1749. https://doi.org/10.1103/physrevb.16.1748

[35] Sa, R. and Liu, D. (2022) Unveiling the Fundamental Physical Properties of $Cu_{2-x}Na_xZnSnX_4$ (X = S, Se) Alloys for Solar Cell Applications: A Theoretical Investigation. *Journal of Materials Research and Technology*, **20**, 2680-2688. https://doi.org/10.1016/j.jmrt.2022.08.070

[36] Prokopidis, K. and Kalialakis, C. (2014) Physical Interpretation of a Modified Lorentz Dielectric Function for Metals Based on the Lorentz-DIRAC Force. *Applied Physics B*, **117**, 25-32. https://doi.org/10.1007/s00340-014-5794-1

[37] Tripathy, S.K. and Kumar, V. (2014) Electronic, Elastic and Optical Properties of $ZnGeP_2$ Semiconductor under Hydrostatic Pressures. *Materials Science and Engineering: B*, **182**, 52-58. https://doi.org/10.1016/j.mseb.2013.11.020

[38] Kumar, M. and Persson, C. (2013) Cu_2ZnSnS_4 and $Cu_2ZnSnSe_4$ as Potential Earth-Abundant Thin-Film Absorber Materials: A Density Functional Theory Study. *International Journal of Theoretical & Applied Sciences*, **5**, 1-8.

[39] Zhao, Y., Li, D. and Liu, Z. (2016) A DFT Study of Pressure-Induced Phase Transitions, Structural and Electronic Properties of Cu_2ZnSnS_4. *Modern Physics Letters B*, **30**, Article ID: 1650176. https://doi.org/10.1142/s0217984916501761

[40] Hall, S.R., Szymanski, J.T. and Stewart, J.M. (1978) Kesterite, $Cu_2(Zn, Fe)SnS_4$ and Stannite $Cu_2(Fe, Zn)SnS_4$, Structurally Similar But Distinct Minerals. *The Canadian Mineralogist*, **16**, 131-137.

[41] Chen, S., Gong, X.G., Walsh, A. and Wei, S. (2009) Crystal and Electronic Band Structure of Cu_2ZnSnX_4 (X=S and Se) Photovoltaic Absorbers: First-Principles Insights. *Applied Physics Letters*, **94**, Article ID: 041903. https://doi.org/10.1063/1.3074499

[42] Ghosh, A., Thangavel, R. and Rajagopalan, M. (2013) First Principles Study of Electronic and Optical Properties of Cu_2ZnSnX_4 (X = S, Se) Solar Absorbers by Tran-Blaha-Modified Becke-Johnson Potential Approach. *Journal of Materials Science*, **48**, 8259-8267. https://doi.org/10.1007/s10853-013-7638-5

[43] Agrawal, A., Meredig, B., Wolverton, C. and Choudhary, A. (2016). A Formation Energy Predictor for Crystalline Materials Using Ensemble Data Mining. 2016 *IEEE*

16*th International Conference on Data Mining Workshops* (*ICDMW*), Barcelona, 12-15 December 2016, 1276-1279. https://doi.org/10.1109/icdmw.2016.0183

[44] König, C., Greer, J.C. and Fahy, S. (2021) Effect of Strain and Many-Body Corrections on the Band Inversions and Topology of Bismuth. *Physical Review B*, **104**, Article ID: 035127. https://doi.org/10.1103/physrevb.104.035127

[45] Zhang, K., Liu, F.Y., Lai, Y.Q., Li, Y., Yan, C., Zhang, Z.A., *et al*. (2011) *In Situ* Growth and Characterization of Cu_2ZnSnS_4 Thin Films by Reactive Magnetron Co-Sputtering for Solar Cells. *Acta Physica Sinica*, **60**, Article ID: 028802. https://doi.org/10.7498/aps.60.028802

[46] Katagiri, H., Sasaguchi, N., Hando, S., Hoshino, S., Ohashi, J. and Yokota, T. (1997) Preparation and Evaluation of Cu_2ZnSnS_4 Thin Films by Sulfurization of E B Evaporated Precursors. *Solar Energy Materials and Solar Cells*, **49**, 407-414. https://doi.org/10.1016/s0927-0248(97)00119-0

[47] Yang, X., Qin, X., Yan, W., Zhang, C., Zhang, D. and Guo, B. (2022) Electronic Structure and Optical Properties of Cu_2ZnSnS_4 under Stress Effect. *Crystals*, **12**, Article 1454. https://doi.org/10.3390/cryst12101454

[48] Nainaa, F.Z., Bekkioui, N., Abbassi, A. and Ez-Zahraouy, H. (2020) First Principle Study of Structural, Electronic Optical and Electric Properties of Ag_2MnSnS_4. *Computational Condensed Matter*, **22**, e00443. https://doi.org/10.1016/j.cocom.2019.e00443

[49] Ito, K. (2015) An Overview of CZTS-Based Thin-Film Solar Cells. In: Ito, K., Ed., *Copper Zinc Tin Sulfide-Based Thin-Film Solar Cells*, Wiley, 3-41. https://doi.org/10.1002/9781118437865.ch1

[50] Butt, M.K., Yaseen, M., Ghaffar, A. and Zahid, M. (2020) First Principle Insight into the Structural, Optoelectronic, Half Metallic, and Mechanical Properties of Cubic Perovskite $NdInO_3$. *Arabian Journal for Science and Engineering*, **45**, 4967-4974. https://doi.org/10.1007/s13369-020-04576-6

[51] Dilshod, N., Kholmirzo, K., Aliona, S., Kahramon, F., Viktoriya, G. and Tamerlan, K. (2023) A DFT Study of Structure, Electronic and Optical Properties of Se-Doped Kesterite Cu_2ZnSnS_4 (CZTSSe). *Letters in Applied NanoBioScience*, **12**, Article 67. https://doi.org/10.33263/LIANBS123.067

[52] Razeghi, M. and Rogalski, A. (1996) Semiconductor Ultraviolet Detectors. *Journal of Applied Physics*, **79**, 7433-7473. https://doi.org/10.1063/1.362677

[53] Rezaei Niya, S.M. and Hoorfar, M. (2013) Study of Proton Exchange Membrane Fuel Cells Using Electrochemical Impedance Spectroscopy Technique—A Review. *Journal of Power Sources*, **240**, 281-293. https://doi.org/10.1016/j.jpowsour.2013.04.011

[54] Chadi, D.J. and White, R.M. (1975) Frequency- and Wave-Number-Dependent Dielectric Function of Semiconductors. *Physical Review B*, **11**, 5077-5081. https://doi.org/10.1103/physrevb.11.5077